Draft version August 22, 2014
Preprint typeset using LaTeX style emulateapj v. 5/2/11

arXiv:1408.4819v1 [astro-ph.EP] 20 Aug 2014

PLANET FORMATION IN STELLAR BINARIES II: OVERCOMING THE FRAGMENTATION BARRIER IN α CENTAURI AND γ CEPHEI-LIKE SYSTEMS

Roman R. Rafikov[1] & Kedron Silsbee[1]

Draft version August 22, 2014

ABSTRACT

Planet formation in small-separation (~ 20 AU) eccentric binaries such as γ Cephei or α Centauri is believed to be adversely affected by the presence of the stellar companion. Strong dynamical excitation of planetesimals by the eccentric companion can result in collisional destruction (rather than growth) of $1-100$ km objects, giving rise to the "fragmentation barrier" for planet formation. We revise this issue using a novel description of secular dynamics of planetesimals in binaries, which accounts for the gravity of the eccentric, coplanar protoplanetary disk, as well as gas drag. By studying planetesimal collision outcomes we show, in contrast to many previous studies, that planetesimal growth and subsequent formation of planets (including gas giants) in AU-scale orbits within ~ 20 AU separation binaries may be possible, provided that the protoplanetary disks are massive ($\gtrsim 10^{-2}M_\odot$) and only weakly eccentric (disk eccentricity $\lesssim 0.01$). These requirements are compatible with both the existence of massive (several M_J) planets in γ Cep-like systems and the results of recent simulations of gaseous disks in eccentric binaries. Terrestrial and Neptune-like planets can also form in lower-mass disks at small (sub-AU) radii. We find that fragmentation barrier is less of a problem in eccentric disks which are apsidally aligned with the binary orbit. Alignment gives rise to special locations, where (1) relative planetesimal velocities are low and (2) the timescale of their drag-induced radial drift is long. This causes planetesimal pileup at such locations in the disk and promotes their growth.

Subject headings: planets and satellites: formation — protoplanetary disks — planetary systems — binaries: close

1. INTRODUCTION.

Planets are known to be able to form in a variety of environments, some of which are believed to be hostile to their genesis. A good illustration of this statement is provided by planets detected in close binary systems, such as γ Cephei (Hatzes et al. 2003). This eccentric ($e_b = 0.41$), relatively small semi-major axis ($a_b = 19$ AU) system consists of two stars of mass $M_p = 1.6M_\odot$ and $M_s = 0.41M_\odot$. It harbors a giant planet with the projected mass $M_{\rm pl}\sin i = 1.6M_J$ in orbit with semi-major axis $a_{\rm pl} \approx 2$ AU and eccentricity $e_{\rm pl} \approx 0.12$ around the primary.

Several more such systems of S-type in classification of Dvorak (1982) are known at present (Chauvin et al. 2011; Dumusque et al. 2012). Two of them — HD 196885 (Correia et al. 2008) and HD 41004 (Zucker et al. 2004) harbor giant planets in orbits with $a_{pl} = 1.6-2.6$ AU. Two more — α Cen (Dumusque et al. 2012) and Gl 86 (Queloz et al. 2000) host planets at smaller separations, $a_{\rm pl} \approx 0.04$ AU and $a_{\rm pl} \approx 0.11$ AU, correspondingly. These systems exhibit a diversity of planetary masses, with an Earth-like planet ($M_{\rm pl}\sin i = 1.1M_\oplus$) orbiting our neighbor α Cen (cf. Hatzes 2013), and other binaries hosting gas giants with $M_{\rm pl}\sin i = (1.6-4.0)M_J$ (Chauvin et al. 2011).

The existence of planets in these tight binaries has been a serious challenge for planet formation theories. The expectation of inner rather than outward planet migration due to disk-planet interaction (Ward 1986) suggests that such planets form in situ, at $1-2$ AU (as we show in this work it is very difficult to form them even further out). At these separations gravitational instability is a very unlikely avenue of planet formation (Rafikov 2005, 2007). An alternative model of core accretion (Harris 1978; Mizuno 1980) relies on formation of a massive core by collisional agglomeration of a large number of planetesimals, possibly starting at small, $\lesssim 1$ km, sizes. It is this stage of planetesimal growth in tight binaries that presents significant problems to existing planet formation theories.

Indeed, it has been known since the work of Heppenheimer (1978) that an eccentric stellar companion can drive very large planetesimal eccentricities, ~ 0.1 at AU-scale separations. This would cause planetesimals to collide at high relative speeds of a few km s^{-1}. As this is much higher than the escape speed from the surface of even a 100 km object (about 100 m s^{-1}), collisions between planetesimals should lead to their *destruction* rather than growth, introducing a *fragmentation barrier* for planet formation (see §4). The theoretical expectation of suppressed planet formation in $a_b < 20$ AU binaries has been largely corroborated by recent observations (Wang et al. 2014).

The premise of our present work is that the key to solving the fragmentation barrier puzzle lies in better understanding of planetesimal dynamics. However, some alternative suggestions have also been considered over the years. For example, Thébault et al. (2008, 2009) proposed that tight planet-hosting binaries could have started on more extended orbits, which were subsequently shrunk by interactions with other stars in their birth cluster. Paardekooper & Leinhardt (2010) propose a solution involving a non-standard mode of planetesimal accretion. It may also be possible that planetesimals are

[1] Department of Astrophysical Sciences, Princeton University, Ivy Lane, Princeton, NJ 08540; rrr@astro.princeton.edu

born big (Johansen et al. 2007), with sizes exceeding 10^2 km, in which case they are safe from collisional destruction from the start. These possibilities would need to be invoked if we were not able to resolve the fragmentation barrier puzzle by the better treatment of planetesimal dynamics alone, underscoring the importance of this aspect of the problem.

Dynamics of planetesimals in binaries are complicated by a plethora of agents affecting their motion. It has been long realized that both the companion gravity and gas drag affect planetesimal motion (Marzari & Scholl 2000; Thébault et al. 2004). However, subsequently it has also been understood that these processes alone cannot overcome the fragmentation barrier (Thébault et al. 2008). More recently, it was shown that the gravity of protoplanetary disk in which planetesimals reside has a dominant effect on their dynamics (Rafikov 2013b; hereafter R13). The tendency of protoplanetary disks in binaries to become eccentric further complicates this issue, see Silsbee & Rafikov (2013; hereafter SR13).

Generalizing these efforts, Rafikov & Silsbee (2014; hereafter Paper I) combined different physical ingredients — gravity of an eccentric disk, perturbations due to the companion star, and gas drag — to present a unified picture of planetesimal dynamics in binaries in *secular* approximation. They came up with analytical solutions for planetesimal eccentricity, and explored the behavior of relative velocities between planetesimals of different sizes.

Our present goal is to use these dynamical results to understand planetesimal growth in tight binaries with particular focus on the fragmentation barrier issue. We couple them with recent understanding of collisional fragmentation based on the work of Stewart & Leinhardt (2009) and explore the conditions under which planetesimals can grow unimpeded by fragmentation in situ, i.e. at the present day orbits of planets in tight binaries. We do this for a variety of different collisional criteria governing planetesimal growth and carefully explore the space of various disk+binary parameters. To summarize our main finding from the start, we find that even in tight binaries planet formation should be possible in *massive* protoplanetary disks which are *only weakly eccentric*.

This paper is structured as follows. We summarize the main dynamical results of Paper I in §3. We describe our treatment of planetesimal collision outcomes in §4. Conditions for planetesimal growth in non-precessing and precessing disks are determined in §5 and §7 correspondingly. Sensitivity of our results to model parameters is explored in §6. Radial migration of planetesimals is covered in §8. Implications of our results for planet formation can be found in §9. We summarize our main conclusions in §10.

2. GENERAL SETUP.

We study planet formation in binaries using a setup similar to SR13 and Paper I. The binary with semi-major axis a_b and eccentricity e_b has components with masses M_p (primary) and M_s (secondary). We define $\nu \equiv M_s/M_p$. The primary star is orbited by an eccentric protoplanetary disk, coplanar with the binary orbit. Fluid elements in the disk follow elliptical trajectories with the primary star in the focus. We adopt a power law dependence of the gas eccentricity $e_g(a_d)$ as a function of the semi-major axis a_d of a particular ellipse:

$$e_g(a_d) = e_0 \left(\frac{a_{\rm out}}{a_d}\right)^q. \quad (1)$$

Here $a_{\rm out}$ is the outer cutoff radius of the disk. Simulations show that in eccentric binaries with $e_b = 0.4$, the disk gets truncated at $a_{\rm out} \approx (0.2-0.3)a_b$ by gravitational perturbations from the companion. Thus, e_0 is the eccentricity of fluid trajectories at the outer edge of the disk, $a_d = a_{\rm out}$.

For simplicity all fluid trajectories are assumed to have *aligned* apsidal lines, so that the disk orientation is uniquely defined via a single parameter ϖ_d — the angle between the disk and binary apsidal lines.

We let $\Sigma_p(a_d)$ be the disk surface density at the periastron of the fluid trajectory with semi-major axis a_d. Surface density at an arbitrary point in the disk can be uniquely specified once $e_g(a_d)$ and $\Sigma_p(a_d)$ are known (Statler 2001; Ogilvie 2001; SR13). Here we assume a power law dependence of Σ_p between $a_d = 0$ and $a_{\rm out}$. Assuming that disk contains mass M_d out to $a_{\rm out}$ the surface density distribution is given by

$$\Sigma_p(a_d) = \frac{2-p}{2\pi}\frac{M_d}{a_{\rm out}^2}\left(\frac{a_{\rm out}}{a_d}\right)^p \approx 3\times 10^3 \text{ g cm}^{-2} M_{d,-2} a_{\rm out,5}^{-1} a_{d,1}^{-1}, \quad (2)$$

where p is the power law index ($p = 1$ in the numerical estimate), $M_{d,-2} \equiv M_d/(10^{-2}M_\odot)$, $a_{\rm out,5} \equiv a_{\rm out}/(5\text{ AU})$ and $a_{d,1} \equiv a_d/\text{AU}$. Equation (2) neglects disk ellipticity and assumes $p < 2$, so that most of the disk mass is concentrated near $a_{\rm out}$. Unless stated otherwise (see §5) we will be using a disk model with $p = 1$ and $q = -1$ in our calculations, i.e. $\Sigma_p(a_d) \propto a_d^{-1}$ and $e_g(a_d) \propto a_d$; see R13 and SR13 for motivation. We assume a disk with $a_{\rm out} = 5$ AU.

Planetesimals of radius d_p orbit the primary within the disk and are coplanar with it and the binary. Their orbits are described by semi-major axis a_p, eccentricity e_p and the apsidal angle (w.r.t. the binary apsidal line) ϖ_p. The latter two are often combined for convenience into the planetesimal eccentricity vector $\mathbf{e}_p = (k_p, h_p) = e_p(\cos\varpi_p, \sin\varpi_p)$. Everywhere in this work we assume $e_p \ll 1$ as well as $e_g \ll 1$.

3. SUMMARY OF THE RESULTS ON PLANETESIMAL DYNAMICS.

In Paper I we obtained a number of important results on the dynamics of planetesimals in binaries in secular approximation, i.e. neglecting short-term gravitational perturbations (Murray & Dermott 1999). Our calculations simultaneously accounted for the gravity of the massive eccentric protoplanetary disk, binary companion, and gas drag.

Gravitational perturbations due to the binary companion and the eccentric disk excite planetesimal eccentricity at the rates determined by the eccentricity excitation terms B_b due to binary and B_d due to disk, given by equations (7,PI) and (8,PI), correspondingly ("PI" means that the referenced equation can be found in Paper I). At the same time, the axisymmetric component of the gravity of these perturbers drives apsidal precession of planetesimal orbits at rates A_b (binary, equation

(5,PI)) and A_d (disk, equation (6,PI)). We invariably find that in disks massive enough to form Jupiter mass planets, $M_d \gtrsim 10^{-2} M_\odot$, planetesimal precession, and often eccentricity excitation, are dominated out to a few AU by the gravity of the disk. This finding is a novel result of R13, SR13 and Paper I.

We showed that in the case of a non-precessing disk with a fixed orientation with respect to the binary apsidal line planetesimal eccentricity $\mathbf{e}_p$ is an analytic function of the planetesimal size d and system parameters, given by the expressions (22,PI)-(28,PI), (32,PI), & (33,PI). The latter enter equations through the two key variables — characteristic eccentricity e_c and size d_c, defined by equations (29,PI) and (31,PI), correspondingly. Dependence of e_c and d_c on the system parameters was explored in great detail.

Our analytic solutions allow us to produce maps of the relative eccentricity $e_{12} = |\mathbf{e}(d_1) - \mathbf{e}(d_2)|$ for pairs of planetesimals of different sizes d_1 and d_2; an example is shown in Figure 1. We also derived a distribution of approach velocities for colliding planetesimals (§8 of Paper I) and shown it to be rather narrow, with the approach velocity v_{12} constrained to lie within the range $(1/2)v_K e_{12} < v_{12} < v_K e_{12}$, where v_K is the local Keplerian speed. Thus, maps such as shown in Figure 1 directly characterize the typical velocity at which planetesimals collide, $v_{12} \sim v_K e_{12}$, and allow us to understand their collision outcomes, see §4.

The e_{12} and v_{12} maps in Figure 1 are made for γ Cephei system at $a_p = 1$ AU for the standard ($p = 1$, $q = -1$) aligned ($\varpi_d = 0$) disk with $M_d/M_p = 10^{-2}$ and $e_0 = 0.03, 0.01$ (resulting in $e_c = 2.45 \times 10^{-3}, 3.15 \times 10^{-4}$ correspondingly). One can clearly see that planetesimals exhibit small relative eccentricity in a blue region around the diagonal line $d_1 = d_2$. This low-e_{12} "valley" appears because planetesimals with similar sizes follow similar orbits, and collide with low relative speed. The valley is narrowest at $d_1, d_2 \sim 0.1 - 1$ km (depending on e_c), which corresponds to the characteristic size d_c given by equation (31,PI). For $d_1, d_2 \ll d_c$ planetesimals experience apsidal alignment and their relative eccentricities are lowered by gas drag. For $d_1, d_2 \gg d_c$, apsidal alignment is accomplished by the disk and companion gravity, again resulting in small e_{12}. On the contrary, planetesimals of very different sizes (upper left and lower right regions) are not aligned and exhibit high relative eccentricity, with $e_{12} \approx e_c$ given by equation (29,PI).

We also obtained some analytical results on planetesimal eccentricity behavior in *precessing* disks, see §6 of Paper I. We did this in two limiting cases: when binary gravity dominates over that of the disk, and vice versa. These asymptotic results are used to understand planetesimal growth in precessing disks in §7.

4. PLANETESIMAL COLLISION OUTCOMES.

Description of the dynamical behavior of planetesimals provided in Paper I is used in this work to understand the outcomes of their collisions.

There are different ways in which planetesimal collisional evolution can be characterized. A high-velocity collision is usually considered *catastrophic* when the mass of the largest surviving remnant is less than half of the combined mass of objects $M_{\rm tot} = m_1 + m_2$ involved. In this work we use a fragmentation prescription developed

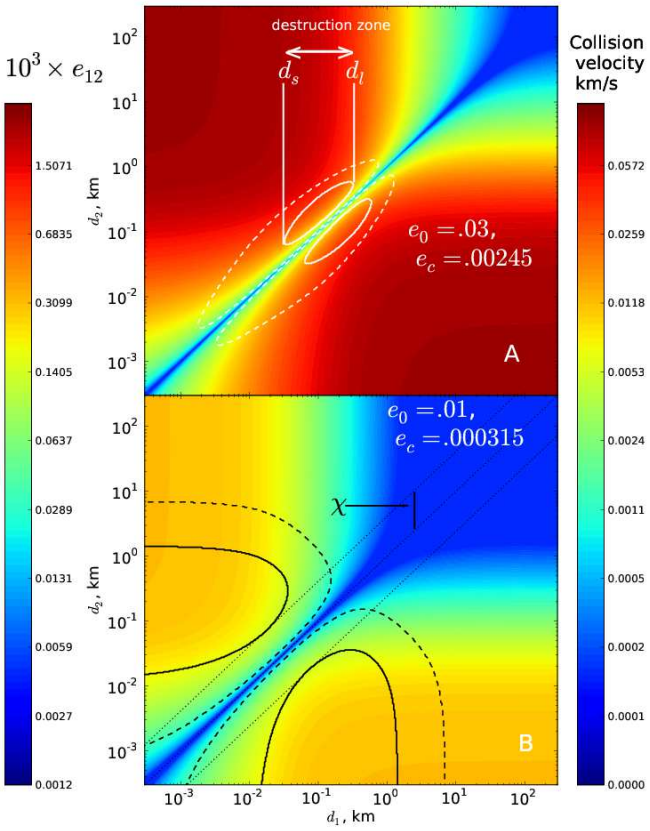

FIG. 1.— Maps of the relative eccentricity e_{12} (left color bar) and velocity $v_{12} = e_{12} v_k$ (right color bar) for planetesimals of different sizes d_1 and d_2 (see Paper I for similar maps). Calculation is done at $a_p = 1$ AU for γ Cephei system for our standard ($p = 1, q = -1$), aligned ($\varpi_d = 0$) disk with $M_d/M_p = 0.01$ and disk eccentricity at its outer edge (a) $e_0 = 0.03$ (resulting in $e_c \approx 2.45 \times 10^{-3}$) and (b) $e_0 = 0.01$ ($e_c \approx 3.15 \times 10^{-4}$). Contours illustrate collisional outcomes using different fragmentation criteria: catastrophic destruction (3) in panel (a) — white, and erosion (6) in panel (b) — black. Planetesimals are destroyed in collisions of pairs of objects within corresponding contours. Solid and dashed contours are for strong and weak planetesimals. The extent of the destruction zone (arrow) and the smallest and largest (d_s and d_l) sizes of planetesimals that get destroyed are illustrated in panel (a). In panel (b) parameter χ measures the extent of the erosion zone: it represents a lower limit on the size ratio of objects that lead to erosive collisions.

by Stewart & Leinhardt (2009), which suggests that a collision is catastrophically disruptive if

$$\frac{Q_{\rm R}}{Q^*_{\rm RD}} > 1, \tag{3}$$

$$Q_{\rm R} = \frac{M_{\rm r} v^2_{\rm coll}}{2 M_{\rm tot}}, \tag{4}$$

$$Q^*_{\rm RD} = q_s R_{C1}^{9\mu_c/(3-2\phi)} v_{\rm coll}^{2-3\mu_c} + q_g R_{C1}^{3\mu_c} v_{\rm coll}^{2-3\mu_c}, \tag{5}$$

where $Q_{\rm R}$ is the appropriately scaled kinetic energy of the collision, $M_{\rm r} = m_1 m_2/(m_1 + m_2)$ is the reduced mass of the colliding objects, and $v_{\rm coll}$ is the collision speed at the moment of contact. The energy threshold for catastrophic disruption $Q^*_{\rm RD}$ depends on constants q_s, μ_c, ϕ, and q_g related to the material properties of the planetesimals; R_{C1} is the radius of a sphere with the mass $M_{\rm tot}$ and a density of 1 g cm^{-3}. Following Stewart & Lein-

hardt (2009), we use $\mu_c = 0.4$, $\phi = 7$, $q_s = 500$, and $q_g = 10^{-4}$ (in proper CGS units) for our weak planetesimals and $\mu_c = 0.5$, $\phi = 8$, $q_s = 7 \times 10^4$, and $q_g = 10^{-4}$ for strong ones.

On the other hand, even if the condition (3) is not satisfied and catastrophic disruption is avoided, collisional growth is not guaranteed — it requires that the largest object (e.g. m_1) is not *eroded* in a collision. Erosion occurs when the largest remnant is less massive than the more massive body involved in a collision. According to Stewart & Leinhardt (2009) erosion happens whenever

$$\frac{Q_{\rm R}}{Q^*_{\rm RD}} > 2\frac{m_2}{M_{\rm tot}}, \qquad m_2 < m_1. \tag{6}$$

This condition is far more prohibitive for growth than (3) since m_2 can be much less than m_1. Growth in a given collision occurs only when the condition (6) is violated.

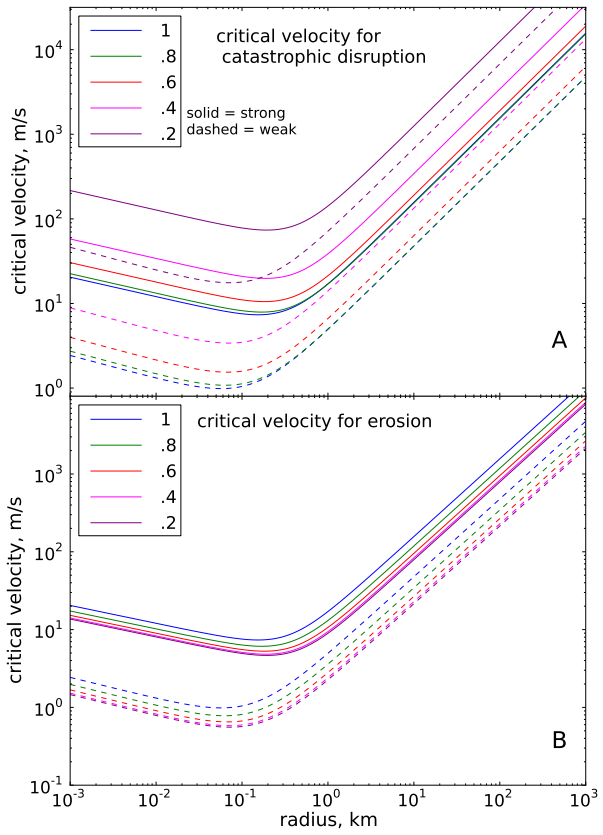

FIG. 2.— Critical velocity curves, shown as a function of the bigger planetesimal radius, for different collisional conditions proposed in Stewart & Leinhardt (2009) and used in this work: (a) catastrophic disruption, equation (3) and (b) erosion, equation (6). Different colors correspond to different size ratios of colliding objects indicated on panels. Solid and dashed curves are for collisionally strong and weak objects, correspondingly.

Figure 2 illustrates the two collisional criteria (3) & (6) by showing the critical (minimum) relative planetesimal velocity $v_{\rm coll}$ that leads to either catastrophic destruction (panel a) or erosion (panel b) of the bodies of different sizes. Various curves correspond to different size ratios and internal strengths of the objects involved in a collision.

In the case of catastrophic disruption critical $v_{\rm coll}$ is a sensitive function of the size ratio of objects involved. Collisions of objects of similar size are clearly more destructive than those of planetesimals with very different sizes as the former are characterized by lower critical $v_{\rm coll}$. For collisionally strong objects (solid curves) we find that most destructive collisions (requiring the lowest relative speed ~ 10 m s^{-1} for destruction of equal mass objects) involve ~ 300 m planetesimals, almost independent of the mass ratio. For collisionally weak objects this size is ~ 100 m and $v_{\rm coll} \sim 1$ m s^{-1} for $m_1 = m_2$.

In the case of erosion critical $v_{\rm coll}$ attains minimum values roughly at the same sizes. However, the dependence on mass ratio is very weak and vanishes in the limit of $m_2 \ll m_1$. This follows from equation (4) that demonstrates that in this limit $Q_{\rm R} \propto m_2$, canceling the dependence on m_2 in the right hand side of the condition (6). This difference in behaviors between the two collisional criteria has important implications as we show next.

We note at this point that critical velocity curves shown in Figure 2b are likely to be not applicable for the case of erosion by very small objects. In this limit one would expect cratering and mass loss from target to be determined by its *local* material properties (Housen & Holsapple 2009), rather than global ones as suggested by the Stewart & Leinhardt (2009) prescription. Then the critical velocity (in the strength-dominated regime, in the absence of ejecta re-accumulation) should become independent of the target size as the projectile-to-target size ratio tends to zero; this is not what Figure 2b shows. To avoid this issue in the following we do not explore erosion in the limit of very large size ratio of colliding bodies, see §5.2.

4.1. *Relative velocities and collision outcomes.*

We now couple this understanding of different collisional outcomes with the dynamical results of Paper I and proceed as follows. We compute the relative collision velocity of the two objects $v_{\rm coll}$ as $v^2_{\rm coll} = e^2_{12} v^2_K + 2G(m_1 + m_2)/(d_1 + d_2)$, where d_1, d_2 are the sizes of planetesimals with masses m_1, m_2. Note that by using the maximum possible approach velocity $e_{12} v_K$ for calculating $v_{\rm coll}$ we are being conservative, since the actual approach speed may be as small as $(1/2) e_{12} v_K$, see §3. The procedure used for calculating relative eccentricity of colliding planetesimals e_{12} in both the non-precessing and precessing disks is outlined in Appendix A.

Maps of e_{12}, $v_{12} = e_{12} v_K$ such as the one presented in Figure 1 show that e_{12} is a function of d_1, d_2, meaning that the same is true for $v_{\rm coll}$ in our approach. We can then use these maps to directly illustrate collision criteria for both strong and weak planetesimals. In Figure 1a the two regions inside the white boundaries stretching along the $d_1 = d_2$ line represent the "zone of destruction": planetesimals with sizes falling into this region get catastrophically destroyed in mutual collisions. The extent of such zone in d_p is indicated with a white arrow, and the largest and smallest planetesimal sizes that get destroyed in collisions are denoted d_l and d_s.

In Figure 1b black contours delineate "zones of ero-

sion": collisions of objects falling within the corresponding contour result in mass loss by the larger planetesimal, hindering growth. The extent of the erosion zone is characterized by the dimensionless parameter χ, which is the *smallest target-to-projectile size ratio of objects that can get eroded* in a collision for a given set of system parameters; see Figure 1b for illustration of this definition. The overall morphology of the erosion zone is similar to "erosion regions" found by Thébault et al. (2008) in $d_1 - d_2$ space using numerical integration of planetesimal orbits and fragmentation criteria different from ours, see their Figures 2, 6, 7. Note however that our Figure 1b shows the erosion zone over much broader range of planetesimal sizes.

Both the "islands of destruction" in Figure 1a and the "islands of erosion" in Figure 1b exhibit a narrow "channel" between them at $d_1 = d_2$, where the growth is possible. This common feature is due to the fact that $e_{12} \to 0$ when d_1 and d_2 are exactly the same, because $\mathbf{e}_p$ is a function of planetesimal size only. At the same time the general morphologies of the destruction and erosion regions are different — the former does not extend too far from the $d_1 = d_2$ line because catastrophic destruction of a target planetesimal in collision of very different objects (either $d_1/d_2 \ll 1$ or $d_1/d_2 \gg 1$) would require very high relative velocity, see Figure 2a. On the other hand, erosion is possible even for collisions of highly unequal objects, see Figure 1b, simply because the critical $v_{\rm coll}$ becomes independent of d_1/d_2 as $d_1/d_2 \to 0$. As expected, for collisionally weak objects both the destruction and the erosion zones are more extended in $d_1 - d_2$ space, as shown by the dashed contours in Figure 1.

The extent of these zones sensitively depends on the value of the eccentricity scale e_c. This is illustrated in Figure 3 where the variation of these zones with the characteristic planetesimal eccentricity e_c is shown for strong planetesimals; the rest of the parameters are as in Figure 1. For high value of the disk eccentricity (at its outer edge) $e_0 = 0.1$ (panel a) one obtains high $e_c \approx 10^{-2}$, which results in very extended destruction and erosion zones. The former zone has $d_l/d_s \approx 300$, while for the latter $\chi \approx 1$. In other words, the growth-friendly channel between the two lobes of the erosion zones is extremely narrow, making planetesimal agglomeration highly unlikely in this case.

Lowering e_0 to 0.03 ($e_c \approx 2.45 \times 10^{-3}$) as in Figure 1a shrinks the size of the destruction zone, so that it presents danger for planetesimals within a size range of only about an order of magnitude, $d_l/d_s \sim 10$. Reducing disk eccentricity even further as in Figure 3b ($e_0 = 8.8 \times 10^{-3}$, $e_c \approx 1.9 \times 10^{-4}$) we find the catastrophic destruction zone to fully disappear.

At the same time, erosion zones tend to persist even in disks with very small eccentricity. For example, one finds $\chi \approx 3$ for $e_0 = 0.01$ ($e_c \approx 3.15 \times 10^{-4}$), see Figure 1b. This means that planetesimals in such a disk cannot erode a larger object if its mass is $\lesssim 30$ times higher. And in Figure 3b, where the destruction zone vanishes completely, the erosion zone with $\chi \sim 10$ is still present and may affect growth of planetesimals with radii $\sim 0.05 - 1$ km.

5. IMPLICATIONS FOR PLANETESIMAL GROWTH IN BINARIES.

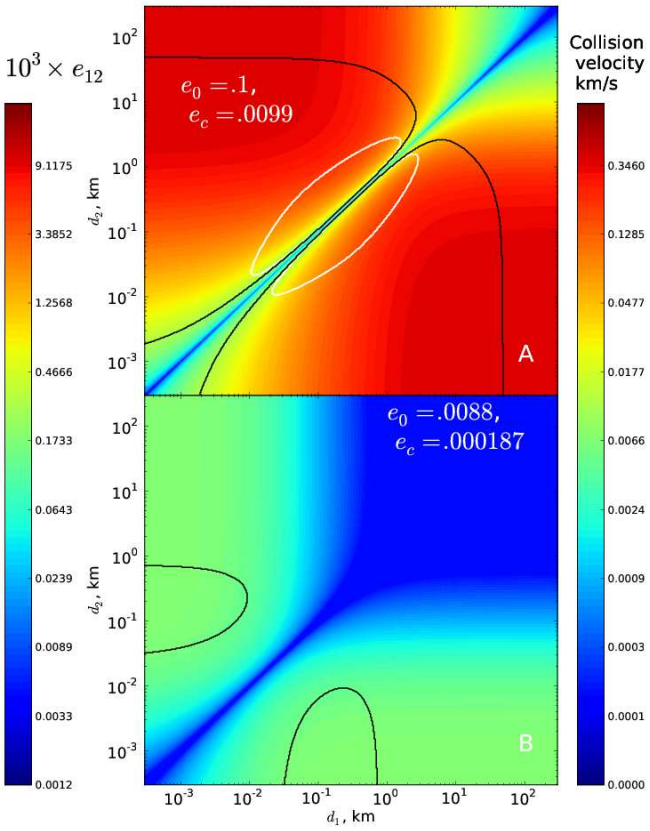

FIG. 3.— Variation of the destruction (white contours) and erosion (black contours) zones with the disk eccentricity and e_c. Calculations are done for the same parameters as in Figure 1, except that now we use (a) $e_0 = 0.1$ (resulting in $e_c \approx 10^{-2}$) and (b) $e_0 = 8.8 \times 10^{-3}$ (resulting in $e_c \approx 1.9 \times 10^{-4}$). Note that in panel (b) catastrophic disruption never presents a problem for planetesimal growth (no white contours).

We now use our understanding of the collisional outcomes described in §4 to explore the possibility of planetesimal growth in binaries as a function of the two key protoplanetary disk characteristics — disk mass M_d and its eccentricity at the outer edge e_0 (defined by equation (1); we fix the disk model to have $p = 1$, $q = -1$).

In Figure 4 we present maps of collisional outcomes for strong planetesimals in the $M_d - e_0$ space. Each map uses parameters of a particular planet-hosting binary — HD196885, γ Cep, and HD 41004 (Chauvin et al. 2011) — selected because they host Jupiter-mass planets in AU-scale orbits. These maps are computed at the distance from the primary a_p equal to the present-day semi-major axis of the planet (shown on panels); planet mass is indicated by the vertical red dashed line in each panel. Calculations used to produce this figure assume that the disk is *aligned* with the binary, i.e. $\varpi_d = 0$. Effect of non-zero ϖ_d is explored further in §6.1.

5.1. *Accounting for catastrophic disruption.*

For each point in the two-dimensional space $M_d - e_0$ we construct the relative velocity distribution for planetesimals of different sizes as shown in Figure 1. Using this map of e_{12} and the recipe provided in §4 we determine whether the catastrophic destruction zone (white

contours in Figures 1 & 3) defined by the condition (3) appears in it. If it does not, then the corresponding points in $M_d - e_0$ space in Figure 4 are colored grey. The resultant grey region in this Figure covers part of the parameter space in which catastrophic collisions do not present a danger to planetesimal growth.

In the opposite case, when the white contours appear in the e_{12} maps, catastrophic disruption gets in the way of planetesimal growth. Parts of $M_d - e_0$ phase space, in which planetesimal growth is interrupted by catastrophic collisions are not colored and lie outside the grey regions in Figure 4.

5.2. *Accounting for erosion.*

Even if catastrophic fragmentation is avoided (i.e. outside of white region in Figure 4), planetesimal growth may still be complicated by the erosion of growing objects in numerous collisions with smaller planetesimals. To address this issue we check whether for given values of M_d and e_0 the erosion condition (6) gets satisfied for any d_1, d_2 in a corresponding map of e_{12} (i.e. whether black contours such as in Figures 1 & 3 appear in the e_{12} map). If it does, we need to decide how dangerous it can be for growth, which is a non-trivial issue.

First, demanding erosion to be *completely absent* as a necessary condition for planetesimal growth is likely too conservative. First, even if some collisions are erosive, planetesimals should still be able to grow provided that the mass gain in non-erosive collisions exceeds the mass loss in erosive impacts. Examination of the erosion zone shape in Figures 1b & 3 shows that a body of a given radius gets eroded predominantly by objects much smaller in size, which may be chipping off relatively small total mass even if erosive collisions are numerous. At the same time, collisions with more massive objects of comparable size result in mergers, adding substantial amount of mass and easily resulting in the net mass gain and overall growth of planetesimals. This can naturally be the case if the planetesimal size distribution is such that at all times most mass is concentrated in largest objects.

The exact balance of mass loss and gain depends on the velocity and mass spectrum of colliding planetesimals. The results of Paper I allow us to predict the former. However, the latter can be known only after a self-consistent calculation of planetesimal coagulation and evolution of the mass spectrum is performed. Such calculation needs to use the improved dynamical inputs from Paper I and requires understanding the inclination distribution of planetesimals in binaries, which is one of the key inputs for calculation of their collision rate. This calculation is beyond the scope of the present work, as our present main goal is simply to understand the general implications of the improved description of planetesimal dynamics (Paper I) on their collisional evolution.

Second, recently Windmark et al. (2012) and Garaud et al. (2013) have shown that planetesimal growth can proceed even in the presence of collisional barriers. This possibility arises when the coagulation-fragmentation process is treated in a *statistical* sense, allowing for a *distribution of collisional outcomes*. Unlike the deterministic approach that is usually employed, this way of treating planetesimal growth allows low probability events — formation of massive objects immune to collisional destruction — to occur, given a large total number of bodies in the system, through a series of "lucky" collisions. As a result, some planetesimals can grow even though the majority get destroyed. In our case this may allow growth if some degree of erosion and even a chance of catastrophic fragmentation (i.e. $d_l/d_s > 1$, see Figure 1a) are present.

To account for these arguments we assume planetesimal growth to be possible in presence of *some erosion*, as long as it is not too significant. More specifically, we will assume that planetesimals can grow (in a statistical sense) if the extent of the erosion zone is limited by some *minimum* value of the parameter χ defined in §4

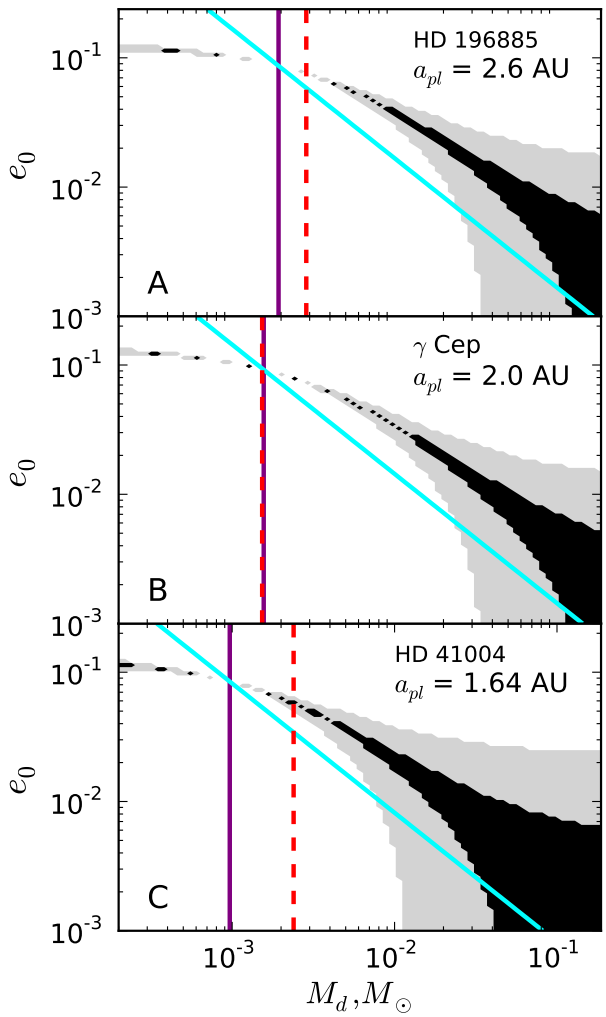

FIG. 4.— Map of the conditions favorable for planetesimal growth in the $M_d - e_0$ space for three binaries (labeled on panels) harboring Jupiter mass planets in orbits with $a_{\rm pl} \sim$ AU. Planetary semi-major axes are indicated and their $M_{\rm pl} \sin i$ are shown with red dashed lines in each panel. Gray areas correspond to disk parameters for which the catastrophic destruction of planetesimals of any size never happens. Black region is a part of phase space where growth with some erosion, limited by the condition $\chi > \chi_{\rm min} = 10^{2/3} \approx 4.6$ (see Fig. 1b) can take place. The purple and cyan lines are the $|A_b| = |A_d|$ and $|B_d| = |B_b|$ conditions, i.e. $M_d = M_{d,A=0}$ and $M_d = M_{d,|B_d|=|B_b|}$ curves defined by equations (49,PI) and (52,PI).

and Figure 1b. In this work, we use a fiducial value

$$\chi_{\rm min} = 10^{2/3} \approx 4.6, \quad (7)$$

which means that a growing planetesimal cannot be eroded in collisions with projectiles more massive than 10^{-2} of its own mass. We choose this particular value of $\chi_{\rm min}$ simply for illustrative purposes, while in practice it should be determined based on planetesimal coagulation models (Windmark et al. 2012; Garaud et al. 2013). It is also low enough that we do not need to worry about the applicability of the critical velocity curves in Figure 2b in the $\chi \to \infty$ limit, see the discussion in §4.

Black regions in Figure 4 cover the part of the $M_d - e_0$ parameter space where the condition $\chi > \chi_{\rm min} = 10^{2/3}$ is fulfilled. We assume planetesimal growth to be possible there, despite some degree of erosion in collisions with small objects.

5.3. *Specific systems.*

A general conclusion that can be drawn from Figure 4 is that, given our growth criteria, planetesimal accretion may be possible in tight binaries at the semi-major axes of the present day planets, as long as the disk mass is high and the disk eccentricity is low. Growth is also possible along a narrow extension of the colored region towards higher e_0 and lower M_d, roughly along the cyan line $|B_d| = |B_b|$ describing the equality of planetesimal excitation by the binary and the disk. The origin of this growth-friendly region is connected to the existence of the valley of stability (see §3) in aligned disks, which is further discussed in §6.1.

Focusing on specific systems, Figure 4c shows that in situ planetesimal growth (i.e. at the observed semi-major axis of the planet) is easiest in the HD 41004 system (Zucker et al. 2004). Planetesimal growth in presence of some ($\chi > 10^{2/3}$) erosion (black region) is possible in this binary even for $M_d \approx 0.02 M_\odot$, as long as $e_0 \lesssim 0.01$. The reason for such favorable conditions lies primarily in the relatively small semi-major axis of the planet, $a_{\rm pl} \approx 1.6$ AU, on which e_c depends very steeply, and the low mass of the primary, $M_p \approx 0.7 M_\odot$, which lowers v_K.

Planetesimal growth is most difficult in HD 196885 system (Correia et al. 2008), see Figure 4a. Previously, Thébault (2011) realized that HD 196885 presents the most serious challenge for in situ planetesimal growth. This is mainly because of the large $a_{\rm pl} \approx 2.6$ AU, making planetesimal accretion with some erosion possible only in very massive disks with $M_d \gtrsim 0.15 M_\odot$ and for $e_0 \lesssim 0.08$. Note that at very high M_d an *evection resonance* corresponding to commensurability $A = n_b$ between the planetesimal apsidal precession and the binary mean motion (Touma & Wisdom 1998), can appear in the disk. This would additionally disturb dynamics of planetesimals and complicate their growth (see Paper I).

Not too different is γ Cephei (Figure 4b) with its high $a_{\rm pl} \approx 2$ AU and $M_p \approx 1.6 M_\odot$: here planetesimal growth with $\chi > 10^{2/3}$ requires $M_d \gtrsim 0.1 M_\odot$ and $e_0 \lesssim 0.007$. Alternatively, growth should also be possible if disk parameters fall within the *valley of stability* (see §6.1), which can be quite wide at its lower right end.

Figure 4 reveals some additional important details. First, purple vertical lines in Figure 4 mark the location of the *secular resonance*, where the planetesimal precession rate $A = A_b + A_d$ becomes zero, see §7.1 of Paper I. At the disk mass $M_{d,A=0}$ corresponding to this resonance (equation (49,PI)) the value of e_c diverges in secular approximation, meaning that planetesimals collide at very high speeds resulting in their destruction.

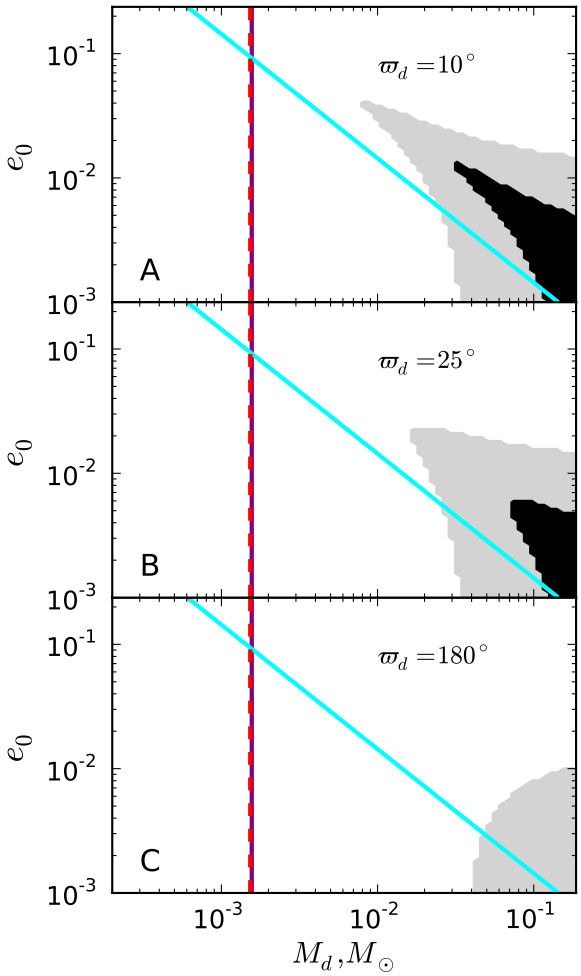

FIG. 5.— Same as Figure 4b (i.e. growth zones in γ Cep) but for a disk misaligned from the binary apsidal axis by an angle ϖ_d indicated on each panel. Note the gradual disappearance of the "valley of stability" and shrinking of the region favorable for planetesimal growth as ϖ_d is increased.

Second, planet masses ($M_{\rm pl} \sin i$) indicated by red dashed lines in Figure 4 never fall below $M_{d,A=0}$ at the corresponding semi-major axis. Under the natural assumption $M_d > M_{\rm pl}$ we can conclude that the protoplanetary disk mass M_d must have exceeded $M_{d,A=0}$ by at least a factor of several. Based on the results of SR13 and Paper I, this inevitably implies that the in situ growth of planetesimal towards forming cores of gas giants should *always proceed in either DD or DB dynamical regimes* in the classification of SR13, i.e. when $|A_d| \gtrsim |A_b|$ (to the right from the purple line in Figure 4) and *disk gravity dominates planetesimal precession rate*. This important fact was completely overlooked prior to the work of R13 and SR13.

6. SENSITIVITY TO MODEL PARAMETERS

Next we explore the sensitivity of our results to the different parameters of the calculation, such as the disk orientation (§6.1), radial distribution of the gas surface density and eccentricity (§6.2), distance from the primary (§6.3). We focus on the γ Cephei system and vary our inputs one by one. The results are then compared with Figure 4b, allowing us to isolate the most important factors affecting planetesimal growth.

6.1. *Role of the disk orientation.*

We start by analyzing how planetesimal growth is affected as we vary the disk orientation with respect to the binary apsidal line, quantified via the angle ϖ_d.

An important feature of the perfectly aligned disk visible in Figure 4b is the *"safe zone"* favorable for growth, which extends towards the upper left corner of the $M_d - e_0$ map. Its origin lies in the presence of the dynamical *"valley of stability"* in the the $M_d - e_0$ phase space for aligned disks. This feature is easily visible in Figure 4a of Paper I as a narrow region, within which characteristic eccentricity e_c is low. Comparing with Figure 4b we see that the shape of the growth-friendly region in $M_d - e_0$ space mirrors the overall morphology of the dynamical valley of stability.

An in-depth discussion of the "valley of stability" properties is provided in §7.2 of Paper I, where it is shown, in particular that for $M_d \gtrsim M_{d,A=0}$ this valley stretches close to $|B_b| = |B_d|$ curve (cyan line in Figures 4 & 5) defined by equation (52,PI), which corresponds to the equality of the planetesimal eccentricity excitation contributions provided by the disk (B_d) and the binary companion (B_b). This dynamical feature makes planetesimal growth possible even in low-mass disks with $M_d \gtrsim 3{\times}10^{-3}M_\odot$ as long as the disk eccentricity e_0 takes on a particular value of order several per cent. The valley of stability vanishes for $M_d \sim M_{d,A=0}$ ($\approx 1.6 \times 10^{-3}M_\odot$ for γ Cep) because a secular resonance appears at this disk mass driving e_c to very high values and making growth impossible. However, for even lower disk masses the valley of stability re-emerges, making planetesimal growth possible even in low mass disks ($M_d \lesssim 10^{-3}M_\odot$) but only at a certain (narrow) range of the disk eccentricity $e_0 \approx 0.1$ given by equation (54,PI).

As the disk orientation changes away from perfect alignment, the valley of stability starts to shrink. Figure 5a shows that even relatively small misalignment of $\varpi_d = 10^\circ$ is enough to eliminate the growth-friendly zone for $M_d \lesssim M_{d,A=0}$. Planetesimal growth without *catastrophic disruption* is then possible only for $M_d \gtrsim 10^{-2}M_\odot$, but it may still proceed at disk eccentricity $e_0 \sim 0.01 - 0.04$ (upper left of the grey region). Growth allowing for *some erosion* with $\chi < 10^{2/3}$ requires $M_d \gtrsim 0.03M_\odot$ and $e_0 \lesssim 0.015$ (upper left of the black region). At the same time the overall morphology of the growth-friendly zone remains roughly the same as in the aligned case — a relatively narrow region extending towards the upper left corner of the $M_d - e_0$ parameter space.

At $\varpi_d = 25^\circ$ growth avoiding the catastrophic fragmentation is possible if $M_d \gtrsim 0.02M_\odot$ and $e_0 \lesssim 0.02$. Erosion with $\chi < 10^{2/3}$ is not an obstacle for growth only for $M_d \gtrsim 0.08M_\odot$ and $e_0 \lesssim 0.006$.

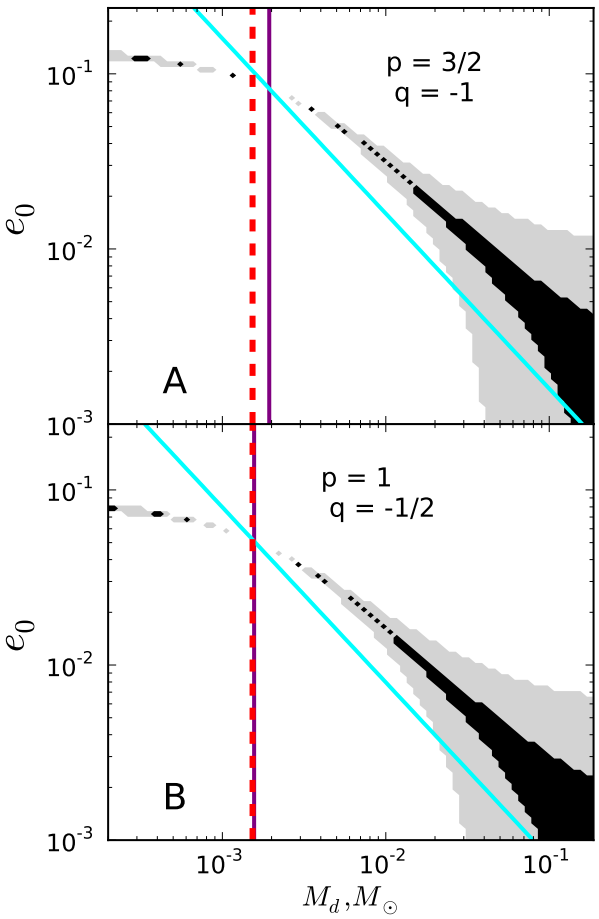

FIG. 6.— Same as Fig. 5a (aligned disk at 2 AU in γ Cephei) but for two different disk models with parameters indicated on panels. For comparison, Fig. 5a uses $p = 1$, $q = -1$.

Finally, for an anti-aligned disk ($\varpi_d = \pi$) the growth avoiding catastrophic destruction is still possible for $M_d > 0.04M_\odot$, $e_0 < 0.01$. Planetesimal growth with even modest erosion ($\chi < 10^{2/3}$) is certainly not possible in such a disk if its mass is below $\sim 0.2M_\odot$.

These results demonstrate that both the valley of stability and the extended region favorable to planetesimal growth in Figure 5 are endemic to relatively well-aligned disks. We conclude that the maximum disk misalignment at which the valley of stability can still facilitate planetesimal growth is $\varpi_d \approx 10^\circ - 15^\circ$.

Simulation results regarding the value of ϖ_d for non-precessing disks are rather mixed. Most of the simulations of Müller & Kley (2012) are consistent with relatively well-aligned disks and $\varpi_d < 10^\circ$. This would greatly facilitate planetesimal growth in binaries. At the same time, Paardekooper et al. (2008) and Marzari et al. (2012) find $\varpi_d \approx \pi$, i.e. anti-alignment. Part of the reason for the discrepancy between the different studies may lie in the method used to determine disk eccentricity (Marzari et al. 2009) — whether it is based on osculating orbital elements of fluid elements or on fitting the isodensity contours of the disk. Thus, the numerical evidence regarding the actual value of ϖ_d is inconclusive at the moment.

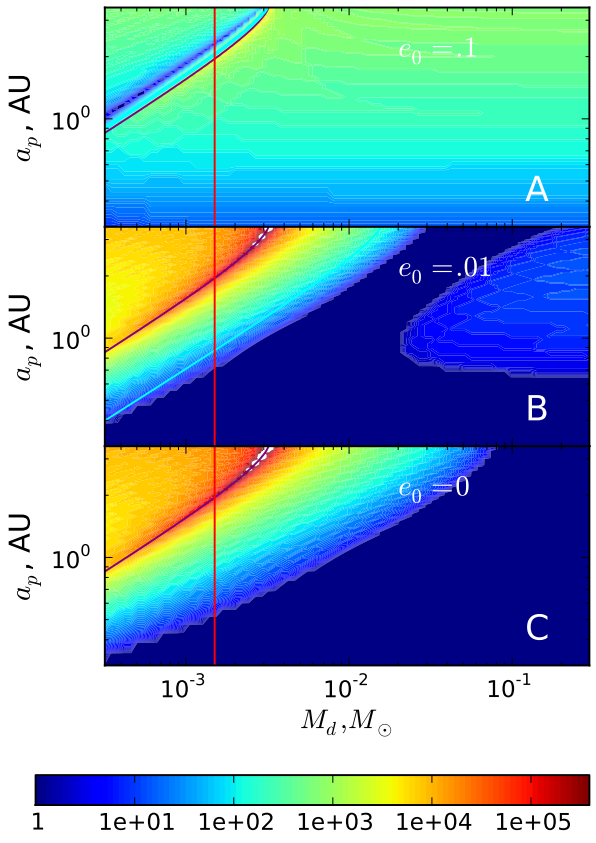

FIG. 7.— Map of the ratio d_l/d_s (see §4) in the $M_d - a_p$ space, illustrating the possibility of catastrophic disruption of planetesimals at different locations in the disk. Calculation is done for an aligned disk ($\varpi_d = 0$) in γ Cep system for three different values of e_0 — the disk eccentricity at its outer edge, indicated on panels. Red line denotes $M_{\rm pl} \sin i$, purple and cyan are the $|A_b| = |A_d|$ and $|B_d| = |B_b|$ conditions.

6.2. *Sensitivity to the disk model.*

In Figure 6 we test the sensitivity of our results on collisional outcomes to other details of the adopted disk model. Namely, we vary power law indices p and q characterizing $\Sigma_d(r)$ and $e_d(r)$. Comparison with the middle panel of Figure 4 shows that variations of the Σ_d profile (i.e. of p) do not induce noticeable changes. However, results are sensitive to the eccentricity profile — the model with $q = -1/2$ ($e_g \propto a_d^{1/2}$) in Figure 6b yields higher disk eccentricity e_g at the same semi-major axis and *for the same* e_0 than the $q = -1$ model ($e_g \propto a_d$), see equation (1). This has detrimental effect on planetesimal growth and shrinks the size of the growth-friendly zone in the $M_d - e_0$ space.

6.3. *Variation with the location in the disk.*

Calculations shown in Figure 4 are performed at a single location — present day semi-major axis of the planet in each system. In Figures 7 and 8 we illustrate how the conditions favorable for planetesimal growth change as the distance to the star is varied.

Our discussion of collisional outcomes in §4 shows that the detrimental effect of catastrophic collisions for planetesimal growth can be characterized by the sizes d_l and d_s of the largest and smallest objects that get destroyed, see Figure 1 for illustration. We can describe the effect of catastrophic collisions via the ratio d_l/d_s, which exceeds unity whenever such collisions are possible for some planetesimal sizes. The higher is d_l/d_s, the more extended is the catastrophic disruption zone and the more difficult it is for growing planetesimals to avoid being destroyed in such collisions. The white regions in maps in Figure 4 correspond to $d_l/d_s > 1$, while in the grey regions catastrophic collisions are absent for any planetesimal sizes.

In Figure 7 we illustrate the sensitivity of planetesimal growth to catastrophic disruption by showing the maps of d_l/d_s as a function of both the disk mass M_d and the semi-major axis a_p, for several values of the disk eccentricity at its outer edge e_0. Calculation is done for an aligned disk in γ Cep system.

For a high $e_0 = 0.1$ we see two regions favorable to growth (i.e. the ones where d_l/d_s is unity or at least less than ~ 10). First, there is a thin dark blue band along the $|B_b| = |B_d|$ (cyan) curve, corresponding to the "valley of stability", see equation (52,PI). Second, close to the star planetesimal dynamics is completely dominated by the disk gravity (DD dynamical regime in classification of SR13), so that $e_c \sim e_g$, which is small in the inner disk (for our $q = -1$).

For the lower eccentricity models shown in panels (b) and (c), most of the DD regime (high M_d, small a_p, see SR13) is favorable for planet formation. It may seem surprising that the $e_0 = 0.01$ case appears to be slightly more favorable than the $e_0 = 0$ case. This is because of the existence of the valley of stability for $e_0 \neq 0$ (panel b), which slightly widens the growth-friendly zone in the DD regime, see §7.2 of Paper I.

It is also interesting that the upper left corner of the high-e_0 map shown in panel (a) is more favorable for planetesimal growth than in maps corresponding to lower e_0. This is caused by the degeneracy of the particular choice $e_0 = 0.1$ mentioned in §7.2 of Paper I (see equation (54,PI)), which causes e_c to be low in the corresponding region (BB regime in classification of SR13) of Figure 4c of Paper I.

Next, in Figure 7 we illustrate the sensitivity of planetesimal growth to *erosion* by showing the maps of $\lg \chi$, where χ is the lowest target-to-projectile size ratio for which erosion is possible for some planetesimal size, see §§4 and Figure 1 for details. Large values of $\lg \chi$ (red) correspond to the situation when erosion occurs only in collisions with very small objects, which do not result in appreciable mass removal from the target. Such collisions are unlikely to prevent planetesimal growth as long as such small objects do not account for the dominant fraction of the disk mass.

One can see that the behavior of $\lg \chi$ in $M_d - a_p$ space largely replicates that of d_l/d_s in Figure 7 — safe zones near the valley of stability, as well as at high M_d and small a_p. Growth-unfriendly regions (blue) lie towards higher a_p and at small disk masses. Thus, planetesimal growth is easiest in massive disks and closer to the star.

7. PLANETESIMAL GROWTH IN PRECESSING DISKS.

In this section we analyze planetesimal growth in disks which do not have fixed orientation with respect to the binary orbit but *precess* at some rate $\dot{\varpi}_d$. We do this

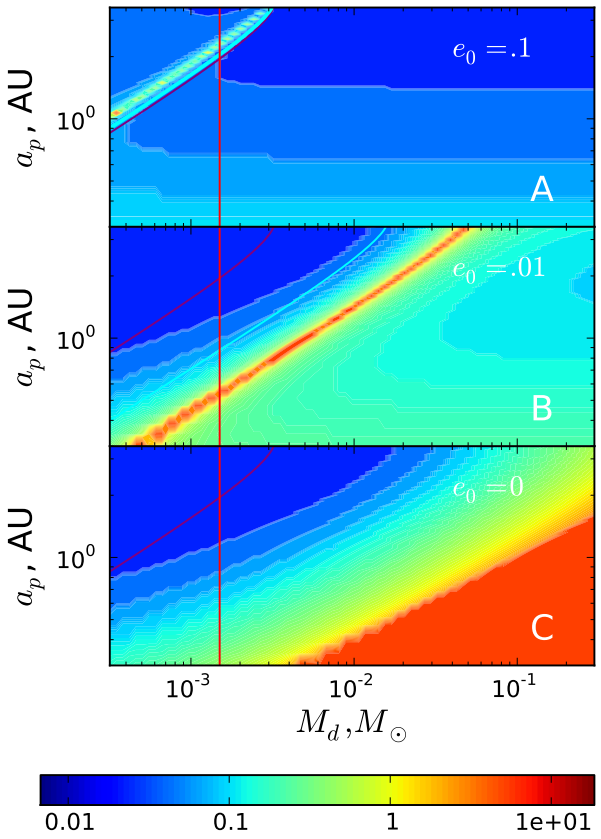

FIG. 8.— Map of the size ratio $\lg\chi$ (see §4) in the $M_d - a_p$ space, illustrating the sensitivity of planetesimal growth to erosion. Note that these are logarithmic maps of $\lg\chi$ (by definition $\chi > 1$, see Figure 1, and the color scheme starts at zero), i.e. yellow corresponds to $\chi \approx 10$, when erosion by objects ≈ 10 times smaller than the target size becomes possible for some planetesimal sizes. The parameters of the calculation and meaning of different curves are the same as in Figure 7.

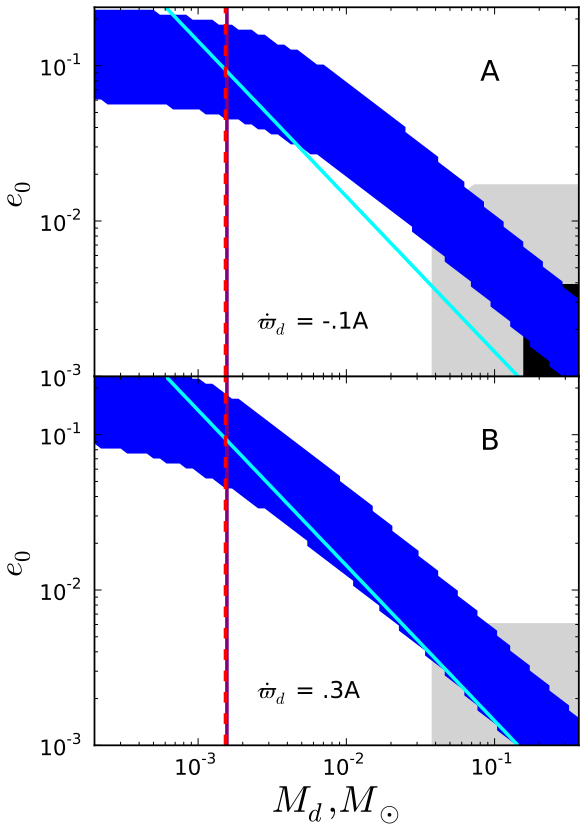

FIG. 9.— Same as Fig. 4b but for a precessing disk with $p = 1$, $q = -1$ around γ Cephei at 2 AU. Disk precession rate is indicated on each panel in units of the local planetesimal precession rate A (which itself depends on M_d within each panel). Analytical description of planetesimal dynamics fails within blue regions, which are excluded from the panels. See text for discussion.

by following the same procedure as in §4, but calculating the relative planetesimal velocity using the results of §6 of Paper I, see Appendix A. Results are shown in Figure 9 where we display regions in the $M_d - e_0$ space favorable for planet formation at 2 AU in γ Cephei for two different values of the disk precession rate $\dot{\varpi}_d$, expressed here in units of the local value of the planetesimal precession rate A. Note that the value of A varies within each panel since it is a function of M_d.

Calculations described in Appendix A for the case of precessing disk do not provide an analytical solution for $|(A - \dot{\varpi}_d)\, e_g + B_d| \sim |B_b|$ (here, again, $A = A_d + A_b$), which excludes certain parts of the $M_d - e_0$ phase space (blue bands) from Figure 9. In the rest of the figure we use the results for strong (§6.1 of Paper I) and weak (§6.2 of Paper I) binary perturbation cases, depending on the circumstances. This makes our treatment of collision outcomes in precessing disk somewhat approximate. Nevertheless, we can understand the main effects of disk precession on planetesimal collisional outcomes by comparing these results with Figure 4b.

First of all, the valley of stability ceases to exist because disk-secondary apsidal alignment is not possible in a precessing disk. This tends to reduce the size of the growth-friendly zone in precessing disks, even far from the center of the valley of stability.

Second, in the strong binary perturbation regime, below the blue band, planetesimal growth conditions are independent of $\dot{\varpi}_d$. This is because the $\mathbf{e}_p$ solutions obtained in §6.1 of Paper I for this regime are independent of $\dot{\varpi}_d$, since eccentricity excitation by the disk is weak. The size of the low-e_0 growth-friendly region varies only because the extent of the excluded region (blue band) depends on $\dot{\varpi}_d$

Third, in the weak binary perturbation regime, above the blue band, the extent of the growth-friendly zone does depend on $\dot{\varpi}_d$. To understand this dependence we recall (see §6.2 of Paper I) that the overall planetesimal eccentricity scale in a precessing disk is given by $e_c^{\rm pr}$, defined by equation (45,PI). Above the blue band $A \approx A_d$, and we can use expressions (6,PI) and (8,PI) for A and $B \approx B_d$. Recalling that for our disk model with $p = 1$, $q = -1$ the coefficients in these expressions are $\psi_1 = -0.5$, $\psi_2 = 1.5$ we can write

$$\frac{e_c^{\rm pr}}{e_g} = 1.5 \left(1 - \frac{\dot{\varpi}_d}{A}\right)^{-1} - 1. \qquad (8)$$

This ratio is equal to 0.5 in a non-precessing disk, when $e_c^{\rm pr} \to e_c$. A simple analysis of equation (8) then shows that $|e_c^{\rm pr}| < e_c$ and non-zero precession *suppresses plan-*

etesimal eccentricity and relative velocity compared to the case of a non-precessing disk if

$$-2 < \frac{\dot{\varpi}_d}{A} < 0. \quad (9)$$

Given that for high M_d, planetesimal dynamics is in the DD regime, for non-pathological disk models (i.e. for surface density slope $0 < p < 3$, SR13) $A < 0$, i.e. planetesimal apsidal precession is *retrograde* relative to its mean motion. Then we conclude from the condition (9) that *slow ($|\dot{\varpi}_d| < 2|A|$) prograde precession of the disk is favorable for planetesimal growth.* This is indeed seen at the high M_d end of Figure 9a, although the magnitude of the effect is small because of the small adopted value of the $|\dot{\varpi}_d/A| = 0.1$ (see below for the characteristic value of $|\dot{\varpi}_d/A|$).

On the contrary, retrograde or fast prograde ($\dot{\varpi}_d > 2|A|$) disk precession *shrinks* the size of the growth friendly zone, as demonstrated by Figure 9b,c for $\dot{\varpi}_d = 0.3A$. This is a bit counter-intuitive as one may naively expect fast precession to result in effective azimuthal averaging of the disk potential, suppressing planetesimal eccentricity excitation by the non-axisymmetric component of the disk gravity, and lowering $|\mathbf{e}_p|$ in agreement with R13 and SR13. However, this argument loses its validity in presence of gas drag, which provides an important contribution to the value of $e_c^{\rm pr}$. For that reason planetesimal growth is facilitated by disk precession only when the somewhat non-trivial condition (9) is fulfilled.

For our fiducial disk with $p = 1$ one finds (R13)

$$|A_d| = n_p \frac{M_d}{M_p}\frac{a_p}{a_{\rm out}} = n_b \left[\frac{(1-\mu)a_b^3}{a_p a_{\rm out}^2}\right]^{1/2}\frac{M_d}{M_p} \quad (10)$$
$$\approx 0.1 n_b \frac{a_{b,20}^{3/2}}{a_{{\rm out},5}a_{p,2}^{1/2}}\frac{M_d/M_p}{10^{-2}},$$

where the numerical estimate is for the γ Cep parameters and $n_b = [G(M_p + M_s)/a_b^3]^{1/2}$ is the mean rate of the binary.

At the same time, simulations of disks in eccentric binaries tend to find a variety of outcomes depending on the detailed physics that goes into the calculations, with both prograde (Okazaki et al. 2002; Marzari et al. 2009) and retrograde (Kley & Nelson 2008; Müller & Kley 2012) precession possible. Numerical results suggest that typically $|\dot{\varpi}_d| \sim (1-2)\times 10^{-2} n_b$ (Marzari et al. 2009; Müller & Kley 2012), which is considerably slower than $|A_d|$ evaluated at the semi-major axis of the planet, $|\dot{\varpi}_d| \sim 0.1|A_d|$. In this case, according to Figure 9a, even if precession is prograde its effect on planetesimal growth in high-mass disks is going to be small (or slightly negative mainly through the elimination of the valley of stability in precessing disks).

Lower mass disks ($M_d \sim 10^{-3} M_\odot$), containing enough mass to form only terrestrial or Neptune-like planets have lower $|A|$. If they precess at the slow rates found in simulations they may have $|\dot{\varpi}_d| \sim |A|$ satisfied. However, as shown in Figure 9, planetesimal growth is strongly suppressed in such low-mass disks. Thus, planetesimal growth in low-mass precessing disks must be rather difficult, at least at separations $\gtrsim 1$ AU. This is contrary to the non-precessing aligned disk case, in which the existence of the valley of stability permits collisional growth even for $M_d \lesssim 10^{-2} M_\odot$, see §5 and Figure 4.

It is also worth noting that simulations with improved treatment of the gas thermodynamics (Marzari et al. 2012; Müller & Kley 2012) and including self-gravity (Marzari et al. 2009) tend to produce *non-precessing* disks, properties of which we explored in previous section. Thus, disk precession is unlikely to strongly affect our conclusions regarding planetesimal growth in S-type binaries.

8. RADIAL MIGRATION OF PLANETESIMALS.

Apart from the eccentricity evolution, the non-conservative gas drag causes inspiral of planetesimal orbits — an effect that was not accounted for in SR13. We now turn our attention to this important issue.

Calculation of the radial drift $\dot{a}_p$ is a more delicate procedure than that of the eccentricity damping. As shown by Adachi et al. (1976), even in the case of a circular disk one has to account for the radial variation of the gas density ρ_g when computing $\dot{a}_p$. Calculation becomes even more complicated in the case of an eccentric disk with its non-axisymmetric surface density profile. Accounting for the difference in azimuthal velocities of gas and particles that results from the radial pressure gradient can be highly non-trivial in the case of an eccentric disk.

For that reason, we have chosen to describe radial planetesimal drift $\dot{a}_p$ using an empirical generalization of the appropriate results of Adachi et al. (1976) for the case of an eccentric disk. This generalization is physically motivated and reduces to the known results in the case of the circular disk with $e_g = 0$. Namely, we use the equation (4.21) of Adachi et al. (1976), in which we simply set $i = 0$ and replace e with the relative particle-gas eccentricity e_r. As a result, we find

$$\dot{a}_p = -\pi \frac{a_p}{\tau_a}\left(\frac{5}{8}e_r^2 + \eta^2\right)^{1/2}\left[\left(\frac{\alpha}{4} + \frac{5}{16}\right)e_r^2 + \eta\right], \quad (11)$$

where

$$\tau_a = e_r \tau_d = \frac{4\pi}{3 C_D {\rm E}\left(\sqrt{3}/2\right)} D^{-1} \quad (12)$$
$$\approx 6 \text{ yr } C_D^{-1}\frac{a_{{\rm out},5}a_{p,1}}{M_{p,1}^{1/2}M_{d,-2}}\frac{h/r}{0.1}d_{p,1}.$$

is the characteristic timescale, τ_d is the eccentricity damping time defined by equation (18,PI), and

$$\eta = \frac{1}{2}(\alpha + s)\left(\frac{c_s}{nr}\right)^2 = \frac{1}{2}\left(p + \frac{s+3}{2}\right)\left(\frac{h}{r}\right)^2 \quad (13)$$

is the measure of the azimuthal particle-gas drift caused by the pressure support in the gas disk. The different parameters entering these expressions are the logarithmic slopes of the gas density and temperature $\alpha \equiv -\partial \ln \rho_g/\partial \ln r$ and $s \equiv -\partial \ln T_g/\partial \ln r$, related via $\alpha = p + (3-s)/2$, see equation (2).

In this work we will use power-law temperature profile $T(r) = T_1 (r/{\rm AU})^{-s}$, with T_1 being the gas temperature at 1 AU, so that

$$\frac{h}{r} \approx 4\times 10^{-2}\left(\frac{M_\odot}{M_p}\frac{T_1}{400\text{ K}}\right)^{1/2}\left(\frac{r}{\rm AU}\right)^{(1-s)/2}. \quad (14)$$

In our calculations we normally take $s = 1/2$ and $T_1 = 400$ K (the central stars of compact planet-hosting binaries are usually somewhat more massive than the Sun).

Note that the characteristic timescale of the radial drift in the case $e_r \gg \eta^{1/2}$ is $|d\ln a_p/dt|^{-1} \sim \tau_a e_r^{-3} = \tau_d e_r^{-2}$, which is much longer than the eccentricity damping time τ_d. For smaller e_r migration time lengthens even further. The slowness of the radial drift allows us to treat a_p as a constant while following the evolution of planetesimal eccentricities.

Radial drift depends steeply on e_r and can be rather fast for strongly dynamically excited planetesimals. Because of the radial pressure support in the gaseous disk resulting in the non-zero value of η, $\dot{a}_p$ does not completely vanish even as $e_r \to 0$. This is not the case for eccentricity evolution — eccentricity damping naturally vanishes for $e_r = 0$.

In Figure 10 we map the migration time $\tau_m \equiv |a_p/\dot{a}_p|$ in M_d-a_p coordinates. We calculate τ_m using equations (11)-(14) for our standard (aligned) disk parameters in γ Cephei for two different values of the disk eccentricity and planetesimal size.

These maps clearly show many non-trivial features and significant variation as we change e_0 and d_p. To better understand them we overplot the lines of $A = 0$ (purple) and $|B_b| = |B_d|$ (cyan) conditions. Interestingly, no significant feature is seen in the τ_m maps at the location of the $A = 0$ secular resonance. This is in contrast to the characteristic eccentricity maps in Figure 4 of Paper I, which show the divergence of e_c at this resonance caused by $e_c \propto |A|^{-1}$ scaling, see equation (29,PI). This difference is easily explained by looking at the equation (28,PI), which shows that the relative planetesimal-gas velocity $e_r \propto |A|e_c$ thus removing singularity at $A = 0$. Upon closer inspection one can see only a mild reduction of τ_m in a broad region surrounding $A = 0$ curve. It is caused by the local $e_r \propto [1+A^2\tau_d^2]^{-1/2}$ dependence on A, increasing e_r and *decreasing* τ_m where $A \to 0$ according to equation (11).

At the same time, in all panels one can easily see a band of *increased* τ_m, which runs close to the $|B_b| = |B_d|$ (blue) curve. Its location is independent of d_p but is sensitive to e_0, with higher disk eccentricity pushing this valley of high τ_m further from the star. Comparing with Figure 4 of Paper I we conclude that this feature is caused by $e_c \to 0$ within this band. Since this is possible only in the aligned disk (see §6.1 and §7.2 of Paper I) such a feature would not be present in a misaligned or precessing disk.

But in a disk with $\varpi_d \approx 0$, migration time can become very long in this region of parameter space: $\tau_m \sim$ Myr is quite typical within the valley of high τ_m stretching along the $|B_b| = |B_d|$ curve, especially for large d_p and higher e_0. In this region e_r can be so small that τ_m becomes determined solely by the non-zero value of η in equation (11), which is due to the radial pressure support in a gas disk:

$$\tau_m \to \frac{\tau_a}{\pi\eta^2} \propto a_p^{7/4} M_d^{-1}. \qquad (15)$$

To arrive at the last scaling we used equations (2), (12)-(14) and adopted $p = 1$, $q = -1$.

Figure 10 shows that τ_m is higher for higher e_0 in high-τ_m regions. This is somewhat counter-intuitive as one naively expects higher disk eccentricity to result in larger planetesimal velocities, driving faster, rather than slower, migration. This contradiction is resolved by understanding that even for the same d_p we are comparing the values of τ_m at special locations, where $e_r \to 0$. Their position is roughly described by equation (52,PI) for $|B_b| = |B_d|$, from which one infers their $a_p \propto (e_0 M_d)^{1/2}$. Plugging this into equation (15) one finds that $\tau_m \propto e_0^{7/8} M_d^{-1/8}$, i.e. maximum τ_m is indeed *longer* for higher disk eccentricity. This is simply a reflection of the fact that for higher e_0 the valley of small e_r moves out to larger a_p. The same reasoning also explains why τ_m increases along the high-τ_m valley as both a_p and M_d get smaller.

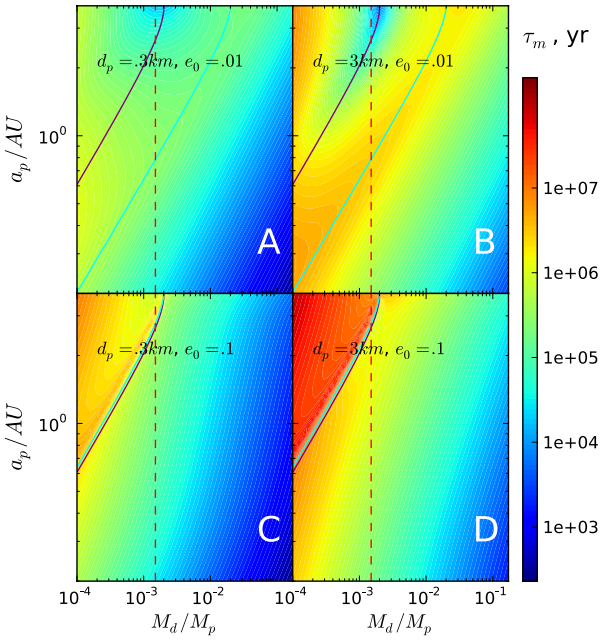

FIG. 10.— Map of the radial drift timescale $|d\ln a_p/dt|^{-1}$ in $M_d - a_p$ space for two different planetesimal sizes, $d_p = 0.3$ km (left) and $d_p = 3$ km (right), and two values of the disk eccentricity at $a_{\rm out}$, $e_0 = 0.01$ (top) and $e_0 = 0.1$ (bottom). Calculation is done for an aligned disk in γ Cephei system.

Note the long values of τ_m in the upper left corner of Figure 10c,d. They are caused by a particular choice of $e_0 = 0.1$ for which e_c becomes very small *globally* in the BB regime, when the gravity of the binary companion dominates over that of the disk (SR13). This coincidence has been previously discussed in §7.2 of Paper I, see equation (54,PI).

Existence of a localized peak of τ_m has important implications for planetesimal growth. In a disk with fixed values of e_0 and M_d, planetesimals in the outer parts of the disk migrate inward until they reach the high-τ_m valley. In a narrow range of semi-major axes corresponding to this valley their radial drift significantly slows down resulting in the local increase of the surface density of solids of different sizes. Given the dramatic local increase of τ_m one can expect planetesimal density there to exceed its initial local value by orders of magnitude. Moreover, according to Figure 4 of Paper I, the high-τ_m valley is also the location where e_c becomes very small providing favorable conditions for planetesimal growth. These points are further discussed in §9.

9. PLANET FORMATION IN BINARIES.

Now we apply our understanding of planetesimal growth and migration described in previous sections to clarify the circumstances under which planets of different masses can form in disks within binaries.

9.1. *Conditions for giant planet formation.*

Presence of planets with $M_{\rm pl}\sin i$ of order several M_J inevitably implies that their parent protoplanetary disks must have been massive, $M_d \gtrsim 10^{-2}M_\odot$: disk mass cannot be much lower than at least several M_J, otherwise disk simply would not contain enough gas to form these massive objects. This argument must hold even despite the observational evidence against massive disks in small separation binaries coming from sub-mm observations (Harris et al. 2012).

Planet masses indicated by the vertical red lines in Figure 4 are no more than an order of magnitude lower than M_d at the edge of the (grey) growth-friendly zone for $e_0 \sim 10^{-2}$. Then, under the natural constraint $M_d \gtrsim 10^{-2}M_\odot$, Figure 4 clearly implies that unimpeded planetesimal growth leading to giant planet formation at AU-scale separations in binaries is *possible provided that disk eccentricity is low*, $e_0 \lesssim 10^{-2}$. This is an important requirement for giant planet formation in small separation ($a_b \approx 20$ AU) binaries, which is inspired by planetesimal dynamics alone. It represents one of the key results of this work.

Unfortunately, we do not have direct measurements of circumstellar disk eccentricities in young stellar binaries and cannot address the e_d constraint directly. Simulations of disks in eccentric binaries with $e_b = 0.4$ tend to find rather low values of $e_d \lesssim 0.05$ (Marzari et al. 2009, 2012; Müller & Kley 2012; Picogna & Marzari 2013). In fact, Regály et al. (2013) claim that for $e_b > 0.2$ protoplanetary disk does not develop permanent eccentricity in their simulations and deviations from axisymmetry are minimal. This is in contrast to simulations of disks in circular (or low-e_b) binaries, which often demonstrate high $e_d \approx 0.3 - 0.5$ (Kley et al. 2008; Regály et al. 2011). Such dychotomy is likely caused by the smaller truncation radii of the disks in high-e_b binaries (Regály et al. 2011) reducing companion perturbation on them. Disks in circular binaries can extend further out, potentially creating conditions for the disk eccentricity excitation via the Lubow (1991) mechanism.

Based on this we conclude that the existing numerical results *are roughly compatible* with the conditions needed for overcoming the fragmentation barrier and forming giant planets within massive disks ($M_d \gtrsim 10^{-2}M_\odot$) in AU-scale orbits, namely, low e_0 of order several per cent, see Figure 4. Note that in very massive disks ($M_d \gtrsim 0.1M_\odot$) this conclusion holds for arbitrary disk orientation as well as in precessing disks, see Figures 5 and 9.

Even in high-M_d disks presence of the valley of stability facilitates planet formation. Figure 10a,b shows that in low-e_0, high-M_d systems the region of long migration time τ_m corresponds to semi-major axis of $2-3$ AU. This means that planetesimals would *preferentially accumulate* at these locations in massive disks by gas-driven radial migration. Corresponding increase of the surface density of solids, combined with the lowered relative velocities of planetesimals at the same locations (see Figure 4), could considerably facilitate growth of planetary cores.

Interestingly, three out of five presently known planet-hosting tight binaries have planets at $a_{\rm pl} = 1.6 - 2.6$ AU, and all three are massive giants with $M_{\rm pl}\sin i > 1.6M_J$ (Chauvin et al. 2011). We suggest that this may be not a coincidence but, possibly, the evidence for in-situ formation of these giants, facilitated by the local pile up of solids, in low-eccentricity ($e_0 \lesssim 0.01$), high mass ($M_d \gtrsim 10^{-2}M_\odot$) disks, which were aligned ($\varpi_d \approx 0$) with the orbits of their binary companions.

We also speculate that the observed clustering of the binary eccentricity in γ Cep-like systems (with $a_b \approx 20$ AU) around $e_b \sim 0.4 - 0.5$ (Chauvin et al. 2011; Dumusque et al. 2012) is directly linked to lower disk eccentricities e_g in them, as suggested by simulations (Regály et al. 2011). These makes such eccentric binaries *more favorable* for overcoming fragmentation barrier and forming planets than their circular counterparts. And in highly eccentric systems, $e_b \to 1$, disks would be truncated at the radii too small to contain enough mass for planet formation. Thus, the apparent clustering of e_b of compact ($a_b \approx 20$ AU) planet-hosting binaries around $0.4 - 0.5$ may be not coincidental.

9.2. *Earth- and Neptune-like planet formation.*

Formation of terrestrial (like in α Cen system, Dumusque et al. 2012) or Neptune-size planets may also proceed in massive disks, in which case the conclusions of §9.1 would apply directly. At the same time, just based on the mass budget, low-mass planets might also be expected to form in lower mass ($M_d \sim 10^{-3}M_\odot$) disks. Sub-mm observations suggest that such disks are more abundant than their more massive counterparts in binaries with separations of order several tens of AU (Harris et al. 2012). However, satisfying the planetesimal growth constraints formulated in §9.1 for low M_d becomes problematic, as can be inferred from the presence of extended growth-unfriendly (white) zones at small M_d in Figure 4. According to Figures 5 and 9 planetesimal growth is essentially impossible in low-M_d disks which are misaligned with the binary orbit or precess.

However, in aligned disks low-mass planet formation may still be possible even for $M_d \lesssim 10^{-2}M_\odot$. In such disks the valley of stability (see Figure 4) provides the conditions favorable for planet formation even for $M_d \lesssim 10^{-2}M_\odot$ and for relatively high $e_0 \sim 0.1$. Moreover, disk evolution may naturally drive even high-M_d systems towards the valley of stability at a given semi-major axis. Indeed, even if the disk starts at relatively high $e_0 \sim 0.1$ and high $M_d \gtrsim 5\times10^{-3}M_\odot$, above the black region in Figure 4, over time its viscous evolutions will reduce M_d and ultimately bring the disk into the valley of stability, making low-mass planet formation quite natural at this point.

Within the localized regions corresponding to the valley of stability one would again have a combination of both the increased density of solids due to planetesimal accumulation induced by the non-uniform planetesimal drift and the suppression of relative planetesimal velocities. Both factors promote planetesimal growth. Figures 7 & 10 clearly show that in low mass disks $M_d \gtrsim 10^{-3}M_\odot$ with relatively high eccentricities $e_0 \sim 0.1$ such low-e_c and high-τ_m regions lie at semi-major axes of 1-2 AU. Earth or Neptune-like planets may form there.

Finally, unimpeded planetesimal growth within rela-

tively low mass disks, $M_d \lesssim 10^{-3} M_\odot$, may also be possible close to the star, at sub-AU separations, provided that the disk has low eccentricity, $e_0 \lesssim 10^{-2}$. This is seen in Figure 7 & 8, which demonstrate small d_l/d_s and relatively large $\lg \chi$ at small a_p. Such mode of planet formation may have been responsible for the origin of the Earth-mass planet in α Cen B (Dumusque et al. 2012).

9.3. *Comparison with previous studies.*

Our finding that fragmentation barrier can be overcome, opening a way to planet formation at separations of several AU in tight binaries such as γ Cep and α Cen is opposite to the conclusions of many previous studies (Thébault et al. 2008,2009; Thébault 2011). The main reason for this difference is in the role of (generally non-axisymmetric) protoplanetary disk gravity, which we account for in secular approximation, while other studies included only gas drag and perturbations from the companion. As we showed in Paper I and in this work this aspect really makes a big difference for the outcome — in disks massive enough to form giant planets, planetesimal precession and eccentricity excitation become dominated by the gravity of the disk rather than of the companion. Thus, it is very important that future studies of planet formation in binaries, including those that self-consistently evolve the disk using direct hydrodynamical simulations, account for the gravitational effect of the disk on planetesimal motion. This has been previously done in Kley & Nelson (2007) and Fragner et al. (2011) but the complexity of planetesimal dynamics including disk gravity has not been explored in sufficient detail in these studies.

On the other hand, some other previous studies have found planetesimal growth in tight binaries to be possible. Marzari & Scholl (2000) arrived at this conclusion by noticing the apsidal phasing of planetesimal orbits by gas drag. But later Thébault et al. (2008) showed the associated reduction of the relative speed v_{12} to be a consequence of a single planetesimal size approximation. Thébault et al. (2006) find growth possible for almost circular binaries with small e_b, since in this case eccentricity forcing by the companion vanishes. However, simulations show that disks tend to develop large eccentricities ($\gtrsim 0.1$) in systems with low e_b (e.g. Marzari et al. 2009,2012; Regály et al. 2011), which, with disk gravity included, would have likely resulted in severe difficulty of forming planets.

10. SUMMARY.

We explored planetesimal growth in AU-scale orbits within small-separation ($a_b \approx 20$ AU) binaries using a newly developed secular description of planetesimal dynamics (Paper I), which includes a number of important physical ingredients relevant for this problem — perturbations due to the companion, gas drag, and, most crucially, gravitational effects of an eccentric disk. We used our results to assess the possibility of planet formation in binaries and arrived at the following conclusions.

- By exploring outcomes of pair-wise planetesimal collisions we identified ranges of planetesimal sizes for which growth by coagulation is suppressed (§4). Inclusion of disk gravity is very important for properly determining the extent of accretion-unfriendly zones.
- Planetesimal growth uninhibited by fragmentation is possible for a broader range of parameters (M_d and e_0) in disks, which are *apsidally aligned* with the binary orbit (§6.1).
- Radial drift of planetesimals caused by gas drag is highly non-uniform in aligned disks, with the drift timescale sharply peaking at AU-scale separations. This causes accumulation of planetesimals at the location where their dynamical excitation is weak and provides favorable conditions for their growth (§8).
- Formation of giant planets in observed (AU-scale) configurations in eccentric binaries like γ Cep is possible in massive and not very eccentric disks, $M_d \gtrsim 10^{-2} M_\odot$ and $e_0 \lesssim 0.01$ (§9.1). The former condition is consistent with the very existence of massive (several M_J) planets in these systems. The latter is in rough agreement with the results of simulations, revealing low disk eccentricity in eccentric ($e_b \approx 0.4$) binaries. Planet formation may be inhibited in circular binaries as simulations show disks to develop high eccentricity in such systems.
- Terrestrial and Neptune-like planets can form in massive disks just as giant planets can. Their genesis in the low-mass ($M_d \lesssim 10^{-2} M_\odot$) disks is possible close to the star ($a_p \lesssim$ AU) but is generally suppressed further out, at $a_p \gtrsim$ AU. However, if the disk and binary periapses are aligned, low mass planets can also form in low-M_d disks at certain locations (even at $a_p \sim$ AU) where the radially migrating planetesimals (1) accumulate and (2) have low relative velocities, promoting their growth in mutual collisions.

Our results provide a natural way of explaining the existence of planets in small separation binaries, such as γ Cep and α Cen, via the improved understanding of planetesimal dynamics. This may eliminate the need to invoke more exotic scenarios for forming such systems.

Our calculations assessed the possibility of planetesimal growth by exploring just the two possible collision outcomes — catastrophic disruption and erosion by objects of certain sizes. The full understanding of planetesimal growth in binaries will require a self-consistent coagulation simulation that would evolve the mass spectrum of objects fully accounting for the complexity of their dynamics in binaries.

Methods developed in this work will be used to understand formation of planets in *circumbinary* configurations.

REFERENCES

Adachi, I., Hayashi, C., & Nakazawa, K. 1976, Prog. Theor. Phys., 56, 1756

Chauvin, G., Beust, H., Lagrange, A.-M., & Eggenberger, A. 2011, A&A, 528, A8

Correia, A. C. M., Udry, S., Mayor, M., Eggenberger, A., Naef, D., Beuzit, J.-L., Perrier, C., Queloz, D., Sivan, J.-P., Pepe, F., Santos, N. C., & Ségransan, D. 2008, A&A, 479, 271
Dumusque, X., Pepe, F., Lovis, C., et al. 2012, Nature, 491, 207
Dvorak, R. 1982, OAWMN, 191, 423
Fragner, M. M., Nelson, R. P., & Kley, W. 2011, A&A, 528, id. A40
Garaud, P., Meru, F., Galvagni, M., & Olczak, C. 2013, ApJ, 764, id. 146
Harris, A. W. 1978, Lunar Planet. Sci., 9, 459
Harris, R. J., Andrews, S. M., Wilner, D. J., & Kraus, A. L. 2012, ApJ, 751, 115
Hatzes, A. P. 2013, 770, id. 133
Hatzes, A. P., Cochran, W. D., Endl, M., McArthur, B., Paulson, D. B., Walker, G. A. H., Campbell, B., & Yang, S. 2003, ApJ, 599, 1383
Heppenheimer, T. A. 1978, A&A, 65, 421
Housen, K. R. & Holsapple, K. A. 2011, Icarus, 211, 856
Johansen, A., Oishi, J. S., Mac Low, M.-M., Klahr, H., Henning, T., & Youdin, A. 2007, Nature, 448, 1022
Lubow, S. H. 1991, ApJ, 381, 259
Kley, W. & Nelson, R. 2007, arXiv:0705.3421
Kley, W. & Nelson, R. P. 2008, A&A, 486, 617
Kley, W., Papaloizou, J. C. B., & Ogilvie, G. I. 2008, A&A, 487, 671
Marzari, F. & Scholl, H. 2000, ApJ, 543, 328
Marzari, F., Baruteau, C., Scholl, H., & Thebault, P. 2012, A&A, 539, id. A98
Marzari, F., Scholl, H., Thébault, P., & Baruteau, C. 2009, A&A, 508, 1493
Mizuno, H. 1980, Progr. Theor. Phys., 64, 544
Müller, T. W. A. & Kley, W. 2012, A&A, 539, id. A18
Murray C. D. & Dermott S. F. 1999, Solar System Dynamics
Ogilvie, G. 2001, MNRAS, 325, 231
Okazaki, A. T., Bate, M. R., Ogilvie, G. I., & Pringle, J. E. 2002, MNRAS, 337, 967
Paardekooper, S.-J. & Leinhardt, A. M. 2010, MNRAS, 403, L64
Paardekooper, S.-J., Thébault, P., & Mellema, G. 2008, MNRAS, 386, 973
Picogna, G. & Marzari, F. 2013, A&A, 556, id.A148
Queloz, D., Mayor, M., Weber, L., et al. 2000, A&A, 354, 99
Rafikov, R. R. 2005, ApJ, 621, L69
Rafikov, R. R. 2007, ApJ, 662, 642
Rafikov, R. R. 2013, ApJ, 764, id. L16
Rafikov, R. R. & Silsbee, K. 2014, arXiv:1405.7054 (Paper I)
Regály, Zs., Sándor, Zs., Dullemond, C. P., & Kiss, L. L. 2011, A&A, 528, id. A93
Silsbee, K. & Rafikov, R. 2013, arXiv:1309.3290 (SR13)
Statler, T. S. 2001, AJ, 122, 2257
Stewart, S. T. & Leinhardt, Z. M. 2009, ApJ, 691, L133
Thébault, P., Marzari, F., Scholl, H., Turrini, D., & Barbieri, M. 2004, A&A, 427, 1097
Thébault, P., Marzari, F., & Scholl, H. 2006, Icarus, 183, 193
Thébault, P., Marzari, F., & Scholl, H. 2008, MNRAS, 388, 1528
Thébault, P., Marzari, F., & Scholl, H. 2009, MNRAS, 393, L21
Touma, J. & Wisdom, J. 1998, AJ, 115, 1653
Wang, J., Xie, J.-W. Barclay, T., & Fischer, D. 2014, 783, id. 4
Ward, W. R. 1986, Icarus, 67, 164
Windmark, F., Birnstiel, T., Ormel, C. W., & Dullemond, C. P. 2012, A&A, 544, id. L16
Zucker, S., Mazeh, T., Santos, N. C., Udry, S., & Mayor, M. 2004, A&A, 426, 695

APPENDIX

RELATIVE ECCENTRICITIES OF PLANETESIMALS

To determine the outcome (destruction or no destruction) of a collision between two bodies of size d_1 and d_2 we need to calculate their relative eccentricity $e_{12} = \left[(h_1 - h_2)^2 + (k_1 - k_2)^2\right]^{1/2}$. In the case of a non-precessing disk we do this by first computing $A\tau_d$ in terms of d_p and d_c for each planetesimal using equation (32,PI), and then plugging it in the equation (64,PI) to find e_{12}.

For the precessing disk (see §7) we do not have analytical expressions for h_p and k_p in general, but we calculate them for two limiting cases (strong and weak binary perturbation cases) using the approach described in §6.1 and 6.2 of Paper I correspondingly. We start by evaluating equation (42,PI). If $|(A - \dot{\varpi}_d)e_g + B_d|$ is within a factor of 2 of $|B_b|$, we exclude this point of the phase space from our calculation as we do not expect analytical limiting behaviors to apply there. If $|B_b| > 2|(A - \dot{\varpi}_d)e_g + B_d|$, then we use equations (43,PI) to determine h_p and k_p. If $|B_b| < 0.5|(A - \dot{\varpi}_d)e_g + B_d|$, then we first compute $(A - \dot{\varpi}_d)\,\tau_d$ using equation (46,PI) and then calculate $\mathbf{e}_p \approx \mathbf{e}_{f,d}$ via equation (B2,PI) with $B_d = 0$ for each planetesimal. Even though k_p and h_p are not constant for a given object (eccentricity vectors precess together with the disk), their difference is constant and is given by

$$e_{12}^2 = e_1^2 + e_2^2 - 2e_1e_2\cos(\phi_1 - \phi_2), \qquad e_i = \left[\frac{e_g^2 + \tau_d^2(d_i)B_d^2}{1 + \tau_d^2(d_i)\,(A - \dot{\varpi}_d)^2}\right]^{1/2}, \tag{A1}$$

where e_i $(i = 1, 2)$ are the individual forced eccentricities for planetesimals of size d_i and ϕ_i are their apsidal phases (with respect to the instantaneous direction of the disk periastron) given by equation (B2,PI)) with $\tau_d = \tau_d(d_i)$.